ELSEVIER

Journal of Magnetism and Magnetic Materials 200 (1999) 456–469

Journal of magnetism and magnetic materials

www.elsevier.com/locate/jmmm

Electronic states in magnetic nanostructures

F.J. Himpsel[a,*], K.N. Altmann[a], G.J. Mankey[b], J.E. Ortega[c,d], D.Y. Petrovykh[a]

[a]*Department of Physics, University of Wisconsin Madison, 1150 University Ave., Madison, WI 53706-1390, USA*
[b]*MINT Center, University of Alabama, Box 870209, Tuscaloosa, AL 35487-0209, USA*
[c]*Dpto. de Física de Materiales, Universidad del País Vasco, San Sebastian, Spain, USA*
[d]*Dpto. de Física Aplicada I, Universidad del País Vasco, San Sebastian, Spain, USA*

Received 12 January 1999; received in revised form 12 March 1999

Abstract

The electronic states responsible for oscillatory magnetic coupling, giant magnetoresistance (GMR), and spin-polarized tunneling are explored. They occupy well-defined locations in $(E, \boldsymbol{k})$ space. Their energy E has to be within a few kT of the Fermi level, a range that is now becoming accessible to high-resolution photoemission. Particular attention is paid to $\boldsymbol{k}$-regions near the Fermi level crossings of the s, p-band, where a sizable group velocity is combined with a d-like magnetic splitting and spin-polarization. These electronic states can be tailored by quantization in structures with single-digit nanometer dimensions, such as two-dimensional quantum wells and one-dimensional arrays of stripes and dots. Such arrays can be produced by self-assembly on top of stepped silicon surfaces.

Keywords: Photoemission; Transition metal; Fermi surface; Quantum well; Spin

1. Introduction

Magnetic nanostructures have opened a variety of avenues for tailoring magnetic materials in the burgeoning field of magnetoelectronics [1–3]. While most of the new devices are still at an exploratory or developmental stage, some of them have made their way into our daily lives. These are spin valves which are used as reading heads in the latest generation of hard disks [4]. The optimum thickness of their active part lies in the single digit nanometer regime. That makes them part of the exclusive, but rapidly growing group of nanostructures that have worked their way into consumer electronics, together with quantum well lasers and MOSFET transistors (containing an ultra-thin gate oxide). For a better understanding of magnetoelectronic devices and for pushing their performance limits it is desirable to know the underlying electronic states. This article gives an overview of what is known about these states from various spectroscopic methods, particularly photoelectron spectroscopy. While our emphasis lies on two-dimensional layer structures and surfaces, we will address one-dimensional stripes and zero-dimensional dots in the outlook. Methods will be explored that make it possible to fabricate stripe- and dot-arrays by self-assembly at stepped silicon surfaces.

* Corresponding author. Tel.: +1-608-263-5590; fax: +1-608-265-2334.
E-mail address: himpsel@comb.physics.wisc.edu (F.J. Himpsel)

0304-8853/99/$ - see front matter
PII: S0304-8853(99)00349-2

1.1. Which states are relevant in magnetoelectronics?

It has been debated for quite some time [5,6], which type of electrons is responsible for the functioning of magnetoelectronic devices. Are the d-electrons or the s, p-electrons responsible for magnetic coupling and spin transport? The band structure of magnetic transition metals contains s, p and d-electrons (Fig. 1). The d-electrons carry a large magnetization and a high density of states, compensated by a low group velocity. Large group velocity of the s, p-electrons, on the other hand, is compensated by a low density of states. A possible solution of this dilemma has been the notion of 'itinerant d-electrons' that exhibit magnetism as well as conductivity [5,6]. Angle-resolved photoemission makes it possible to pinpoint these states in energy and momentum space [7,8] (Fig. 2). Only electrons near the Fermi level E_F contribute to magnetic coupling, conductivity,

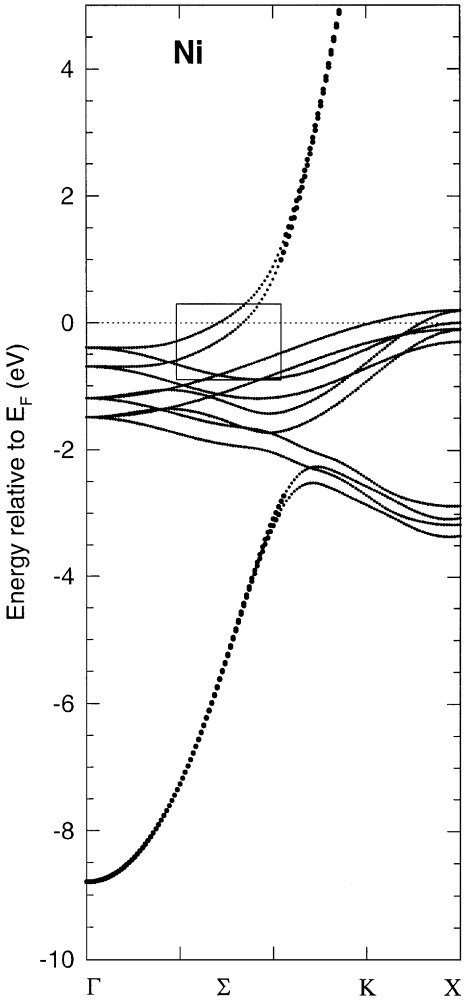

Fig. 1. Empirical $E(\boldsymbol{k})$ band dispersions of Ni along the [1 1 0] direction (Σ line). Bands with more than 50% s, p-character are shown in bold. A parabolic s, p-band crosses a set of flat d-bands and hybridizes with them, forming an avoided crossing. Carriers located at the Fermi level crossing of this hybrid band (box) are likely to dominate magnetic transport properties.

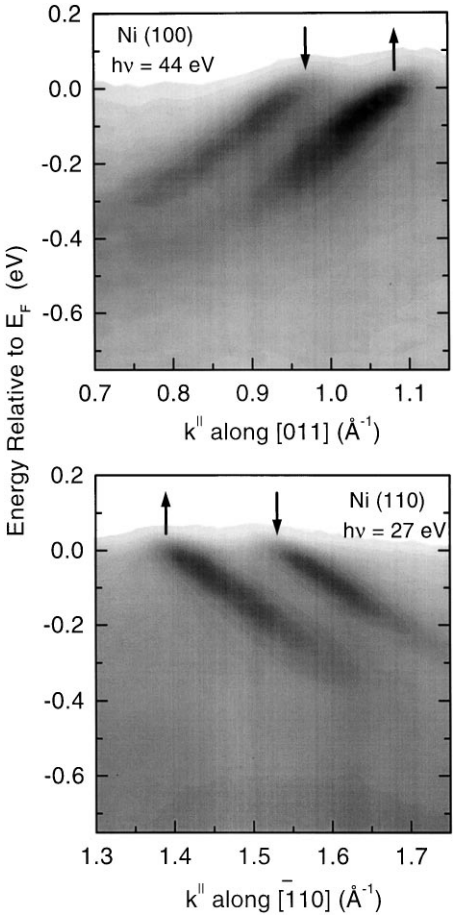

Fig. 2. Experimental $E(\boldsymbol{k})$ relations for Ni, obtained from a high resolution spectrometer with (E, ϑ) multidetection. The (E, $\boldsymbol{k}^{\|}$) region shown covers part of the Σ-axis highlighted by a box in Fig. 1. It contains the Fermi level crossing of the s, p-band, hybridized with the d_z^2-band. This $\boldsymbol{k}$-region is accessible from the Ni(1 0 0) surface (top) and, in reverse, from the Ni(1 1 0) surface (bottom). Dark regions represent high photoemission intensity.

magnetoresistance, and spin-polarized tunneling. Therefore, we focus on resolving the Fermi level crossings of the s, p and d-bands with a resolution better than the thermal energy kT. Particularly interesting will be the region where the s, p-band crosses E_F and flattens out to become d-like (see the box inside Fig. 1). At this point we find both, a sizable magnetic splitting and a substantial group velocity, suggesting that this part of the Fermi surface represents the 'itinerant d-electrons'.

1.2. Tailoring electronic states by nanostructuring

Magnetism as cooperative phenomenon lends itself to manipulation in small structures, where neighbor atoms can be replaced systematically by species with stronger or weaker magnetism. For example, we will discuss layer structures where the magnetic coupling and the magnetoresistance can be modified in controlled fashion by varying the thickness and sequence of the layers. Again, electrons at E_F play the crucial role, and the important parameters are their density of states and their spin-dependent scattering. The former triggers magnetic phase transitions and determines the coupling in multilayers, the latter causes magnetoresistance.

Fig. 3 shows how the density of states at E_F can be manipulated by creating quantum well states in nanostructures. For the example in Fig. 3 we have taken a one-dimensional quantum well (a wire) that creates discrete states out of a continuum at $k^{\|}$, with

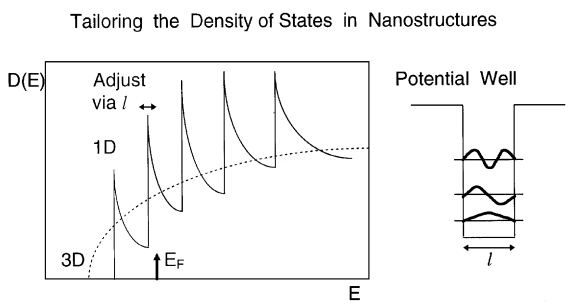

Fig. 3. Schematic of how confinement to a nanostructure can be used to modify the density of states at the Fermi level E_F. Quantum well states lead to maxima in the density of states. These can be swept through E_F by varying the width l of the quantum well (see Eq. (1)).

$k^{\|}$ being the wave vector parallel to the wire. After adding the kinetic energy $(\hbar k^{\|})^2/2m$ along the wire one obtains sub-bands whose density of states diverges like $1/\sqrt{E}$ at the bottom of each sub-band. One of these singularities can be aligned with E_F by choosing an appropriate width l of the well, because the energies of the quantum well states scale like $1/l^2$. For the difference between the lowest two quantum well states in an infinitely deep well one obtains

$$\delta E_{1,2} = 3h^2/8ml^2. \quad (1)$$

If one wants a quantum device to be used at room temperature there is an upper limit for the length l: the spacing between adjacent quantum well states has to be large compared to the thermal energy $kT = 0.025$ eV. Otherwise the discrete structure of the energy spectrum would be blurred when integrating over all the relevant electrons within a few kT of E_F. The criterion $\delta E_{1,2} \geqslant 0.025$ eV gives the condition $l \leqslant 7$ nm, leading us to structures in the single digit nanometer regime.

2. Characterization of electronic states

Electrons in a solid are completely characterized by a set of quantum numbers. These are energy, E, momentum $\hbar\boldsymbol{k}$, point group symmetry (i.e., angular symmetry), and spin. This information can be summarized by plotting $E(\boldsymbol{k})$ band dispersions with the appropriate labels for point group symmetry and spin. Localized electronic states exhibit flat $E(\boldsymbol{k})$ band dispersions, such as 4f levels of rare earths. In the following we will focus on band-like, or itinerant magnetism, which is characteristic of s-, p-, and d-levels in transition metals and rare earths. A complete set of quantum numbers is obtainable from photoemission [9] and inverse photoemission [10], its time-reversed counterpart (electron in, photon out). The former probes occupied states, the latter unoccupied. The local electronic states in magnetic nanostructures are accessible via scanning tunneling spectroscopy [11,12]. In this case, a distribution of momenta around the direction normal to the surface is sampled. While spin-resolved versions of photoemission [13–15] and inverse photoemission

[16] have been available for some time, a spin-polarized version of scanning tunneling spectroscopy is still in its infancy [17].

2.1. $E(\boldsymbol{k})$ from photoemission and inverse photoemission

Photoemission and inverse photoemission provide just the right number of independent variables for establishing a unique correspondence to the quantum numbers of an electron in a solid. The energy E is obtained from the kinetic energy of the electron. The two momentum components parallel to the surface, $\boldsymbol{k}^{\parallel}$, are derived from the polar and azimuthal angles of the electron (ϑ and φ). The third momentum component, $k^{\perp}$, is varied by tuning the photon energy $h\nu$, e.g., using synchrotron radiation. The polarization of the photon provides the point group symmetry and the spin polarization of the electron the spin quantum number.

For two-dimensional states, such as surface states and quantum well states, the determination of energy bands is almost trivial since only E and $\boldsymbol{k}^{\parallel}$ have to be determined. We start with the observed energy E_u and parallel momentum $\boldsymbol{k}_u^{\parallel}$ of the upper state (the emitted photoelectron or the incoming electron in inverse photoemission):

$$|\boldsymbol{k}_u^{\parallel}| = (2mE_u)^{1/2}/\hbar \sin\vartheta$$
$$= 0.51\ \text{Å}^{-1} \cdot \sqrt{E_u\,(\text{eV})} \sin\vartheta. \quad (2)$$

The energy E_l and parallel momentum $\boldsymbol{k}_l^{\parallel}$ of the lower state that one wants to determine are given by conservation laws:

$$E_l = E_u - h\nu, \quad (3)$$

$$\boldsymbol{k}_l^{\parallel} = \boldsymbol{k}_u^{\parallel} - \boldsymbol{g}^{\parallel}. \quad (4)$$

$h\nu$ is the photon energy and $\boldsymbol{g}^{\parallel}$ a vector of the reciprocal surface lattice (zero for most clean metal surfaces). For bulk states we need the perpendicular momentum $k^{\perp}$. It is not conserved when the electron crosses the surface barrier, requiring more elaborate methods [9]. At high enough electron energy (typically >20 eV) the upper state can be approximated inside the solid by the parabolic band of a free electron, shifted by an inner potential V_0. That provides an additional equation for determining $k^{\perp}$:

$$E_u \approx \hbar^2 \boldsymbol{k}_u^2/2m + V_0$$
$$= 3.81(\text{eV})(\boldsymbol{k}_u^{\parallel 2} + k_u^{\perp 2})(\text{Å}^2) + V_0. \quad (5)$$

A typical value of V_0 is -10 eV (relative to the vacuum level). Here we use $V_0 = -9$ eV for Fe and $V_0 = -10$ eV for Ni, together with work functions Φ of about 5 eV. For transitions between bulk states one has full $\boldsymbol{k}$ conservation inside the solid, therefore

$$k_l^{\perp} = k_u^{\perp}. \quad (6)$$

A simple graphical scheme for obtaining bulk bands, including Fermi surface (Fig. 4), is produced when these equations are applied to photoemission data, such as those in Figs. 2 and 5. The kinetic energy for states at the Fermi level is $E_{kin} = E_u = (h\nu - \Phi)$ where $h\nu$ is the photon energy. E_{kin} and the polar angle ϑ of the photoelectrons determine $\boldsymbol{k}_l^{\parallel}$ via

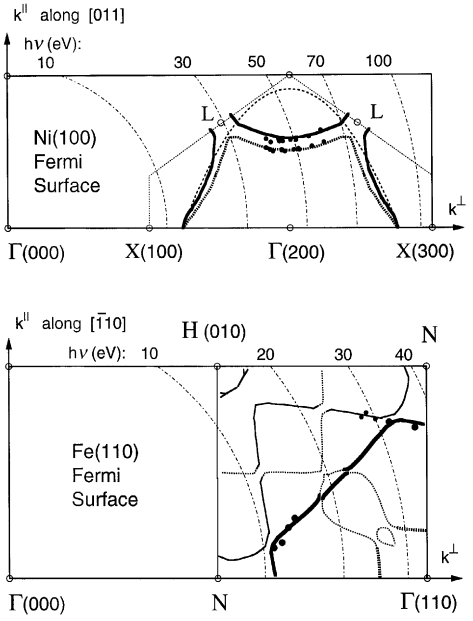

Fig. 4. Fermi surfaces of the s, p-band in Ni and Fe, obtained from photoemission (symbols) and de Haas van Alphen data [74] (lines; minority spins dotted). The component parallel to the surface $\boldsymbol{k}^{\parallel}$ is measured directly (Eq. (4)). The perpendicular component $k^{\perp}$ is obtained via a free-electron upper band (Eq. (5)) which constrains the location of $\boldsymbol{k}$ to the dot-dashed circles for various photon energies $h\nu$. The s, p-like portion of the Fermi surface (bold) can be identified by its high group velocity and by its roughly spherical shape centered around Γ.

Eq. (2). The condition for $k_1^{\perp}$ in Eqs. (5) and (6) gives a circle that intersects the $\boldsymbol{k}_1^{\parallel}$ line at a well-defined point. A series of such points, taken at different $h\nu$, produces the Fermi surface in Fig. 4. The accuracy of the nearly free electron approximation for the upper band can be tested by symmetry checks and by taking data from surfaces with different crystallographic orientations, such as those shown in Fig. 2. Here the Fermi level crossing of the s, p-band along the Σ line is observed from two different crystal surfaces. For the Ni(1 0 0) surface the photon energy $h\nu = 44$ eV has been chosen such that one maps out an arc in $\boldsymbol{k}$-space close to the Σ line from Γ at (2, 0, 0) for $\boldsymbol{k}^{\parallel} = 0$ to X at (2, 1, 1) for $\boldsymbol{k}^{\parallel} = [0\ 1\ 1]$ (in units of $2\pi/a$). For the Ni(1 1 0) surface at $h\nu = 27$ eV one moves in the reverse direction from X at (1, 1, 0) for $\boldsymbol{k}^{\parallel} = 0$ to Γ at (0, 2, 0) for $\boldsymbol{k}^{\parallel} = [\bar{1}\ 1\ 0]$.

The experimental bulk bands of the elemental ferromagnets Fe, Co, Ni, and Gd have been mapped, and the results have been fitted by empirical band structures $E(\boldsymbol{k})$ analogous to the one shown in Fig. 1 (for details see Refs. [3,21,22]. They are all characterized by a steep s, p band crossing a region of flat d-bands. Gd has additional 4f levels that have a dispersion too small to be measured (< 50 meV). Another distinction between s, p, d, and f states is provided by their cross-sections. For example, s, p-bands dominate at low photon energies (below 10 eV) and d-bands at higher energies [22,23]. The f states in rare earths turn on at higher energies yet (above 30 eV). These cross-sections are determined by the match between the wavelength of the photoelectron and the radius of the orbital. Higher angular momentum states have a smaller radial quantum number and require photoelectrons with a shorter wavelength for a match.

2.2. Magnetic splitting and spin polarization

The magnetic exchange splitting δE_{ex} between majority and minority spin bands is the key to magnetism. It is responsible for the difference in filling between the majority and minority spin band that produces the magnetic moment. Therefore, one might expect the moment to increase with the exchange splitting [24,25]. For example, the values of δE_{ex} in Fe, Co, and Ni are 1.8–2.4 eV, 0.93–1.05 eV, and 0.17–0.33 eV [25]. The corresponding moments are 2.2, 1.7, 0.6 μ_B. Because of their high density of states and large magnetic splitting the d electrons carry most of the moment (about 110%), whereas the s, p-electrons are weakly polarized in the opposite direction (about -10% of the total moment). However, the s, p-band acquires a substantial magnetic splitting as it hybridizes with a d-band when approaching E_F (see Fig. 1). For example, the splitting measured in Fig. 2 is 0.23 eV, close to the 0.3 eV typical of a d-band in Ni.

The spin polarization at E_F is crucial for spin transport, such as in giant magnetoresistance and spin-polarized tunneling. As the atomic number decreases from Cu to Ni, Co, and Fe, the uppermost d-band moves up through E_F. Ni has only about half of the upper minority spin d-band above E_F, whereas in Fe the topmost minority spin d-band is completely empty and the corresponding majority spin band has moved partially above E_F. That produces a net minority spin polarization at E_F in Ni and Co and majority spin polarization at E_F in Fe. Even though the s, p-band has an overall (energy-integrated) polarization opposite to the d-bands, it always exhibits majority spin polarization at E_F. That is to be expected from a free-electron-like band with monotonically increasing density of states. These qualitative considerations can be backed up by quantitative results from calculated bands, projected onto different angular momentum states [3,26]. As a result of such non-trivial behavior of different bands at E_F, the analysis of giant magnetoresistance and spin-polarized tunneling has mostly been restricted to simple, parabolic band approximations [27–34].

Taking realistic energy bands, the distinction between s, p and d states becomes blurred. They hybridize since the spherical symmetry of the atom is broken by the $\boldsymbol{k}$-vector. Even along high symmetry directions there is mixing, for example, between s, p_z and d_z^2 states in the Σ_1-band that crosses the Fermi level along the [1 1 0] direction in FCC and BCC structures (Fig. 1). The steep section of this band is usually labeled the s, p-band because it tracks a free-electron parabola for a significant portion of $\boldsymbol{k}$-space. However, near the Γ-point the Σ_1 band is mostly d-like, with a large exchange

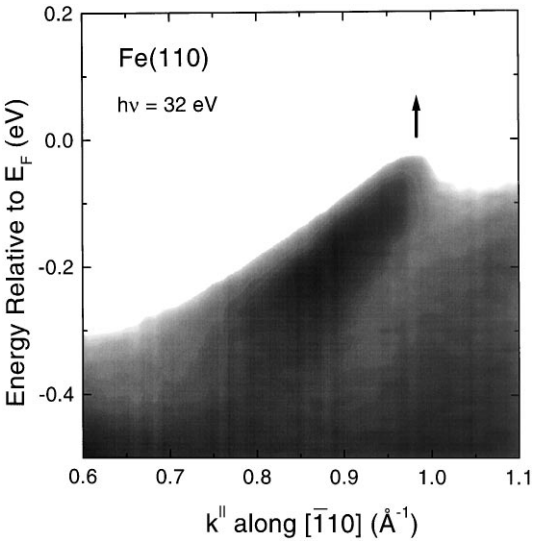

Fig. 5. Photoemission data of the Fermi level crossing of the majority spin s, p-band in Fe(1 1 0) along the [$\bar{1}$ 1 0] azimuth.

splitting δE_{ex} and flat band dispersion. The Fermi level lies near the cross-over from s, p-like to d-like, giving the band a highly mixed character. A quantitative projection onto the different angular momenta is somewhat dependent on the calculation method and the normalization volume, but it produces at least as much d-character as s, p-character for the Σ_1 band at E_F. In the empirical band calculation of Fig. 1 the Σ_1 band is already more d-like at E_F than s, p-like. Therefore, these Fermi level crossings of the s, p-band deserve to be labeled itinerant d-bands [5,6]. We will give a variety of arguments below suggesting that electrons in this type of band are the carriers responsible for magnetoresistance and tunneling. They also dominate magnetic coupling across a non-magnetic spacer layer, as long as it is more than a few atomic layers thick.

2.3. Lifetime and mean free path from linewidths

Spin transport is not only controlled by the density of states at E_F, but also by the scattering time τ, as one can see by expressing the conductivity σ of a metal as a function of the carrier density n:

$$\sigma = ne^2\tau/m. \quad (7)$$

While the s, p band provides the carriers, the d-bands make their presence felt as scatterers. They determine the lifetime τ and mean free path $\lambda = v_F \cdot \tau$ of s, p-electrons at E_F. Below the Fermi level the scattering time decreases rapidly due to the increasing volume of energy and momentum space available for creating electron hole pairs. For example, the energy bands in Fig. 2 are only sharp within 0.2 eV of E_F and broaden quickly at lower energies to become invisible on this scale. This emphasizes once more the need for high resolution measurements close to E_F.

In most ferromagnets the scattering is stronger for minority spin electrons, leaving majority spin s, p-electrons as the principal carriers. The reason is the high density of minority spin d states at the Fermi level in 'strong' ferromagnets, where the top of the majority spin d-band lies below E_F (separated by the Stoner gap [3] Δ, which is 0.11 eV in Ni and 0.35 eV in Co). Since low-energy electron–electron scattering processes are essentially spin conserving, minority spins are affected the most. Magnetic impurities alter the spin dependence of the scattering length dramatically [35,36], offering possibilities for manipulating GMR devices by magnetic 'doping'. For example, there are indications that the minority spin scattering length is reduced from 40 Å in Ni to 6 Å by admixing Fe in permalloy (see below). The opposite effect can be achieved by admixing Cr to Ni, that is majority spins are scattered more strongly than minority spins, giving rise to a reverse GMR effect [37]. A similar doping effect occurs at interfaces: placing a high-moment ferromagnet at the interfaces of a spin valve increases the spin dependence of the interface scattering. For example, interface doping of a permalloy/Cu/permalloy structure by Co more than doubles the magnetoresistance [38,39]. The impurity states at E_F responsible for this effect are just beginning to be explored, and element-specific techniques will become critical, such as MCD, resonant photoemission, and core level fluorescence. Systematic studies exist for monolayer and interface states of transition metals that might be connected with spin-dependent interface scattering [40–43].

Sophisticated multilayer structures allow an analysis of the spin-dependent bulk mean free paths

at the Fermi level via GMR experiments [30,31]. Typical values range in 2–10 nm, with a spin asymmetry ranging from 10 in Co to <1 in Fe, where the majority/minority spin ratio at the Fermi level is inverted relative to Co and Ni. Noble metals, such as Cu, have a much longer mean free path of >100 nm at the Fermi level. The mean free path for spin-flip scattering usually is much longer. Typical values [44–47] range from μm in noble metals to tens of nm in metals with spin impurities as spin scatterers.

High resolution photoemission experiments can assist in determining lifetime and scattering length. The lifetime τ is given by the energy broadening δE:

$$\tau = 1/\delta\omega = \hbar/\delta E \tag{8}$$

where δE is the full width half maximum of a Lorentzian and τ the time constant of an exponentially decaying intensity. The energy broadening leads to a $\boldsymbol{k}$-broadening via the $E(\boldsymbol{k})$ band dispersion:

$$\delta E = \partial E/\partial \boldsymbol{k} \cdot \delta \boldsymbol{k} = \hbar \boldsymbol{v}_{\mathrm{F}} \cdot \delta \boldsymbol{k}. \tag{9}$$

The k-broadening δk, in turn, gives rise to a finite scattering length (= mean free path)

$$\lambda = 1/\delta k. \tag{10}$$

Experimental fits to Lorentzians are given for Ni and permalloy in Fig. 6. From an image, such as Fig. 2, one can extract momentum distributions $I(k^{\parallel})$ at constant energy $E = E_{\mathrm{F}}$ and energy distributions $I(E)$ at constant momentum $k^{\parallel}$. Such cuts are indicated by horizontal and vertical lines in the images. The energy resolution is 9 meV for the Ni spectra (6 meV for photons and 6 meV for electrons) and the angular resolution $\pm 0.15^0$, which translates into a $k^{\parallel}$ resolution of 0.01 $\mathrm{\AA}^{-1}$ at $h\nu = 44$ eV. The width of the lines in Ni ($\delta k_{\uparrow} = \delta k_{\downarrow} = 0.05$ $\mathrm{\AA}^{-1}$) can be attributed mainly to effects not related to the scattering length, such as structural/thermal disorder, and lifetime broadening of the upper band.[1] In permalloy, however, δk is spin-dependent [8] ($\delta k_{\downarrow} = 0.24$ $\mathrm{\AA}^{-1}$ versus $\delta k_{\uparrow} = 0.11$ $\mathrm{\AA}^{-1}$). That suggests a lifetime contribution of 0.13–0.24 $\mathrm{\AA}^{-1}$ to $\delta k_{\downarrow}$, depending on whether all or none of the observed $\delta k_{\uparrow}$ is attributed to the

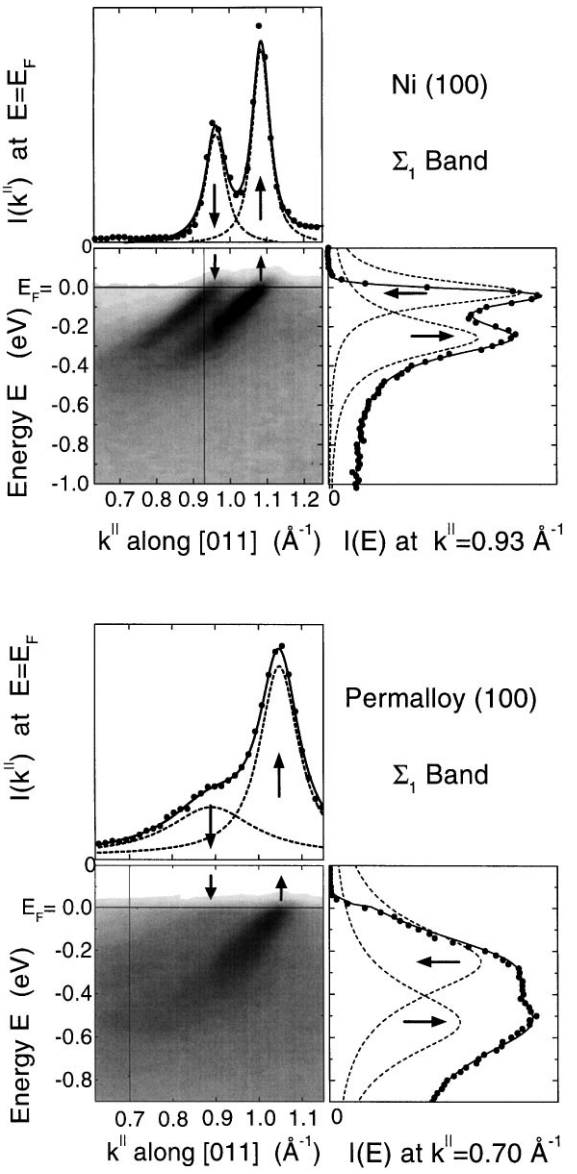

Fig. 6. Photoemission from the Fermi level crossing of the Σ_1 s, p-band in Ni and permalloy ($Ni_{0.8}Fe_{0.2}$), together with cuts along constant E and $\boldsymbol{k}$. Lorentzian fits provide lifetimes and scattering lengths (Eqs. (8)–(10)). Majority and minority spins are denoted by up and down arrows.

[1] The experimental geometry has been chosen such that $k^{\perp}$ broadening in the upper band (due to the finite escape depth) is minimized. The Fermi surface is tangent to the surface normal at this $\boldsymbol{k}$ point, eliminating $k^{\perp}$ broadening in lowest order.

spurious effects mentioned above. The resulting scattering length $\lambda_\downarrow$ of 4–8 Å is extremely short.[2] This value is consistent with some of the results from GMR structures [48–51] ($\lambda_\downarrow \leqslant 6$ Å at room temperature, 10 Å at 4 K, 6 Å at 1.5 K). Determining the mean free path from the momentum broadening makes it possible to extend transport measurements to shorter λ values where GMR structures would have to be just a few atomic layers thick and require atomically abrupt interfaces. In photoemission the solid vacuum interface is utilized, which is always atomically sharp.

2.4. Many-electron effects

In addition to the single-electron band states there exist many-electron excitations in transition metals. The classic example is a satellite in the photoelectron spectrum at 6 eV below E_F in Ni that is due to the excitations of two d-electrons [52–54]. It takes away spectral weight from the single-particle bands all the way up to the Fermi level and thus affects the states relevant to magnetoelectronics. For example, it reduces the magnetic splitting δE_{ex} of the d-bands by a factor of 2–3 and reduces the d-bandwidth by up to 40%, thereby reducing the Fermi velocity. Furthermore, minority states lose more spectral weight at E_F than majority states, contributing to an anomalously high spin polarization [7,8] at the Fermi level in Ni. The two-electron satellite is strongest in Ni and becomes weaker towards Co and Fe [52–54]. The distortions of the single-electron bands at E_F become smaller as well. This can be explained by the weakening of the nuclear potential when reducing the atomic number, which reduced the localization of the 3d states and diminishes d–d interactions. The d–d interactions are even stronger when going beyond Ni towards Cu, but the 3d states have moved 2 eV below E_F and have less influence on the band structure at E_F. There are few empty 3d states left for a second d-electron to get excited into. Therefore, the two-electron satellite becomes weaker again in Cu [52–54].

3. Electronic states in magnetoelectronics

In order to understand magnetic transport phenomena, such as magnetoresistance, spin-polarized tunneling, and the spin transistor we have to know the charge and spin carriers in magnetic materials. It is clear that the relevant electronic states have to lie close to Fermi level, e.g., within a few kT in conductance and a few tenths of an eV in planar tunneling through insulators, vacuum tunneling, and field emission, depending on the barrier height [55]. Beyond that there is no obvious answer. Are these the s, p-electrons or the d-electrons? Are they majority spin or minority spin? The argument for transport by s, p-electrons is based on their high Fermi velocity $\boldsymbol{v}_F = \hbar^{-1} dE/dk$. The d-bands are flatter, with a low group velocity and high effective mass. For example, we find $\boldsymbol{v}_F = 3 \times 10^5$ m/s at the Fermi level crossing of the s, p-band in Figs. 1 and 2, which is higher than the $\boldsymbol{v}_F$ of the d-band crossings near the X-point in Fig. 1. Likewise, we find $\boldsymbol{v}_F$ to be about three times as large for the s, p-band in Fe than for a nearby d-band (Fig. 5, large dots versus small dots in Fig. 4, bottom).

Regarding the spin polarization of the current one might be tempted to argue that the highly polarized d-electrons with their large total density of states dominate. That would give a net minority spin current in Ni and Co where the majority spin d-bands are full (compare the d band Fermi level crossings near the X-point in Fig. 1, which have minority spin character). However, majority spin polarization has been found in spin-polarized tunneling from ferromagnets into superconductors [32]. Likewise, the reduction of the resistance in GMR (negative magnetoresistance) is described by models where the majority spin current exceeds the minority spin current [27–31] (Section 3.2). Again, the majority spin polarization of the s, p-band at E_F resolves this dilemma if s, p-states are taken as the spin carriers.

[2] The anomalously-short scattering length of minority spins in permalloy shows up not only in the $I(k^{\parallel})$ distribution, but also in the $I(E)$ spectrum (right side of Fig. 6). In elemental ferromagnets the peak closer to E_F is higher due to its smaller lifetime broadening, reflecting the strong energy-dependence of the lifetime (see the $I(E)$ spectrum of Ni in Fig. 6). In permalloy that peak height is lower due to the strong scattering of minority spins at E_F.

In the following, we will elaborate on the electronic states that are responsible for specific phenomena in magnetoelectronics, i.e., oscillatory coupling, GMR, and spin-polarized tunneling.

3.1. Oscillatory coupling: quantum well states

Can quantum well states modify the electronic and magnetic structure of a material, as suggested in Fig. 3? This idea becomes reality [56–61] for the oscillatory magnetic coupling between two magnetic layers that are separated by a noble metal. Fig. 7 compares long-period oscillations in the magnetic coupling [62][3] with density of states oscillations [56,57] for FCC Co(1 0 0)/Cu(1 0 0) sandwiches. Both have the same period of about 6 monolayers (1.1 nm). Such an agreement is found wherever comparable data exist [3], e.g. for Ag/BCC Fe(1 0 0), Au/BCC Fe(1 0 0), Cu/FCC Co(1 0 0), Cu/FCC Fe(1 0 0), Cr/BCC Fe(1 0 0). Different periodicities correspond to different points in $\boldsymbol{k}$ space for the quantum well states. For example, there are two oscillation periods in the Co/Cu/Co(1 0 0) system. The long, 6 monolayer period in Fig. 7 is derived from the belly of the Fermi surface at $\boldsymbol{k}^{\parallel} = 0$. A short, 2.7 monolayer period (see footnote 3) originates from the neck of the Fermi surface at finite $\boldsymbol{k}^{\parallel}$ (Fig. 8).

The connection between quantum well states and magnetic coupling can be made rigorous by calculating the total energy of all occupied quantum well states and minimizing it between the two magnetic configurations [58–61]. The density of states at E_F jumps periodically with increasing thickness, whenever a new quantum well state crosses the Fermi level. Here we restrict ourselves to a qualitative discussion, where we consider the charge and spin density wave generated by the envelope wave function of a quantum well states [3,56,57]. It is shown schematically in Fig. 7 (top right). A more realistic view of the spin density wave has been obtained from first-principles band calculations [64] (Fig. 7, bottom). Inside the Cu spacer layer the calculated spin density has the p_z, d_z^2 character expected from the s, p-band and d_z^2-band hybrid. These states transmit the spin information from one magnetic layer to the other. For transmitting magnetic information they must be spin polarized, even in a noble-metal spacer such as Cu. This rather counter-intuitive picture of a 'magnetized' noble metal is confirmed by spin-polarized photoemission [65–67] (Fig. 8) and by magnetic circular dichroism [68,69].

The explanation for the spin polarization of quantum well states is based on a spin-dependent electron reflectivity of the interfaces, an effect that also plays a role in GMR (Section 3.2). In a simple interferometer picture, quantum well states are standing waves created by reflection of electrons at the interfaces (Fig. 7). The reflectivity at a ferromagnetic interface differs between majority and minority spins, because of the magnetic exchange splitting of the bands. For the short-period quantum well states in Co/Cu/Co(1 0 0) there is a gap in the minority spin bands of Co. Therefore, minority spins are totally Bragg reflected at the interface. Majority states, on the other hand, exist on both sides of the interface and are able to propagate. This leads to discrete quantum well states with minority spin character, superimposed on a continuum of bulk-like majority spin states (Fig. 8). In general, there is not such a clear distinction between the reflectivity of majority and minority spins. However, one can argue that there will be a spin-dependent potential step at the interface that makes the reflectivity spin dependent. For spacer layers to the right of the ferromagnets in the Periodic Table, the majority bands are more closely aligned than the minority bands, because of a better match in band filling. This explains the observation of quantum well states with minority spin in noble metals. The situation is reversed for spacers to the left of the ferromagnets, such as Cr, and one expects quantum well states with majority spin character. Quantum well states have been observed in Cr, [70] but their spin polarization has not yet been measured.

3.2. GMR: spin-dependent scattering

The GMR effect is based on spin-dependent scattering, either in the bulk or at interfaces [27–31].

[3] For more recent data including short-period oscillations see Ref. [63].

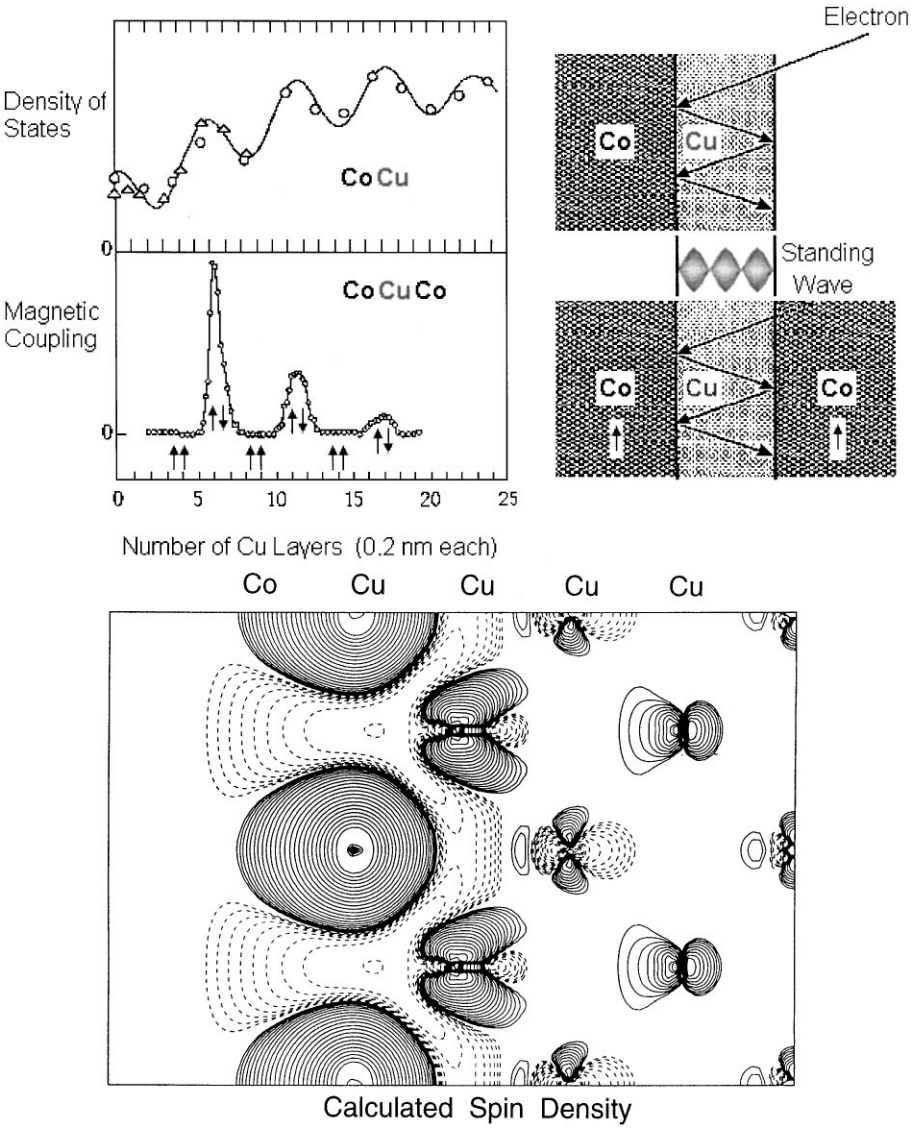

Fig. 7. Oscillatory magnetic coupling in Co/Cu/Co(1 0 0) driven by quantum well states at E_F. The long-period oscillations observed via the Kerr effect (from Qiu et al. [62]) are synchronous with the density of states maxima [56,57] created by quantum well states at the belly of the Cu Fermi surface. A calculation of the spin density wave introduced by all quantum well states is given on the bottom (from Wu and Freeman [64]).

That can be seen rather clearly by considering the fundamental unit in GMR structures, such as spin valves. A pair of ferromagnetic layers is separated by a non-magnetic spacer. The ferromagnetic layers and their interfaces act as spin filters for electrons, based on the different scattering probabilities in the bulk and at the interface: for parallel magnetization of the two ferromagnets we have parallel spin filters with a high transmission, for antiparallel magnetization the spin filters are opposite to each other and block the current. An external magnetic field switches the configuration from antiparallel to parallel, thereby reducing the resistance.

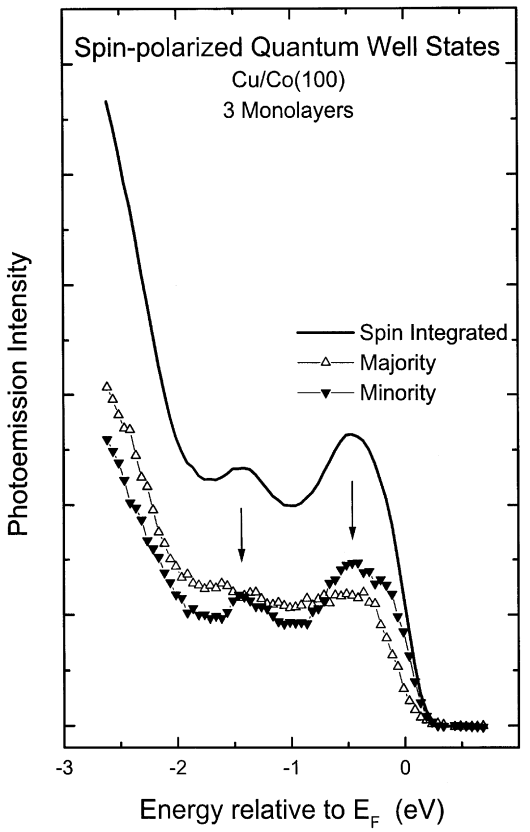

Fig. 8. Spin-resolved photoemission spectra of short-period quantum well states in Cu/Co(1 0 0) that are derived from the neck of the Cu Fermi surface ($h\nu = 77$ eV, $\vartheta = 11^0$ along [0 1 1]). Minority spins are reflected at the interface and confined to the Cu layer, giving rise to peaks for discrete quantum well states (arrows). Majority spins are transmitted and preserve the continuous, bulk-like spectrum.

The spin-dependent reflectivity of electrons at interfaces that gives rise to spin-polarized quantum well states is expected to play a role in GMR as well. In fact, experiments with multilayers of the same overall thickness but different number of periods suggest that there is a strong interface component to the GMR effect [71]. Likewise, the strong effect of interface doping on GMR [38,39] points towards the interface. Interface scattering also causes the GMR to be larger in the CPP geometry (conductivity perpendicular to the plane) than in CIP (conductivity in-plane) where electrons can bypass the interfaces. The question remains whether the spin-dependent interface scattering in GMR is specular, as for quantum well states, or diffuse.

The contribution of the bulk to GMR is caused by the different scattering lengths for minority and majority spins. We have seen in Section 2.3 that a large bulk asymmetry may develop in alloys, such as permalloy, where the minority scattering length is only 6 Å versus a majority scattering length of 40 Å.

3.3. Spin-polarized tunneling: polarization at E_F

Spin-polarized tunneling can occur between various combinations of ferromagnets, normal metals, and superconductors [32–34]. In all cases there is an insulating spacer layer that acts as barrier for planar tunneling. The effective barrier quickly increases for electrons tunneling at energies below E_F, letting only electrons within a few tenths of an eV below E_F participate in tunneling. Of those, the s, p-electrons with their more delocalized wave functions leak out the farthest and are expected to dominate the tunneling matrix element. As mentioned earlier, d-electrons would give the wrong sign for the spin polarization in Ni and Co. A simple free electron model for the s, p-electrons [5,6,32] cures this flaw. Integrating the constant density of states in three-dimensional $\boldsymbol{k}$-space over the Fermi sphere $|\boldsymbol{k}| \leqslant k_F$ one obtains a total s, p-electron density $N \sim k_F^3 \sim E_F^{3/2}$ and a density of states $n = \mathrm{d}N/\mathrm{d}E \sim E_F^{1/2} \sim k_F$. The corresponding spin polarization at E_F is:

$$P_{\mathrm{Free}} = [(n_\uparrow - n_\downarrow)/(n_\uparrow + n_\downarrow)] = [(k_{F\uparrow} - k_{F\downarrow})/(k_{F\uparrow} + k_{F\downarrow})]. \quad (11)$$

That fits the data [32] for Fe quite well ($P_{\mathrm{Tunnel}} = 40\%$ versus $P_{\mathrm{Free}} = 43\%$) and it did fit early results for Ni. However, the experimental spin polarization in Ni has increased substantially as better tunnel junctions became available [32,72,73] and is now incompatible with the free electron model ($P_{\mathrm{Tunnel}} = 23 - 33\%$ versus $P_{\mathrm{Free}} = 6\%$ when using de Haas van Alphen and photoemission data [8] for k_F).

This discrepancy in Ni calls for a more refined model. First one should take the actual Fermi surface with its $\boldsymbol{k}$-dependent magnetic splitting into

account, instead of using a free-electron Fermi surface with a constant splitting. Fig. 4 shows portions of the Fermi surfaces of Ni and Fe derived from de Haas van Alphen data [74] (lines), together with photoemission results (symbols) obtained from data similar to those in Figs. 2 and 5. Portions of the Fermi surface have been assigned to the s, p-band (bold lines, full symbols). Thereby we have selected the bands that exhibit the largest Fermi velocities and are closest to a free-electron sphere.

In addition to the correct Fermi surface one has to take the actual spin polarization at E_F into account. As pointed out in Section 2.4, many-electron excitations may selectively remove spectral weight from the minority spin band, thereby enhancing the spin polarization. This effect is strongest in Ni and fades with decreasing atomic number towards Co and Fe. It might explain why the density-of-states model in Eq. (11) works best for Fe and worst for Ni. The spin polarization at E_F can be observed indirectly in high-resolution photoemission experiments by resolving the two spin components at E_F and determining their area ratios (see Fig. 6, top panels). From the Ni(1 0 0) data [8] in Figs. 2 and 6 we obtain an area ratio $A_\uparrow/A_\downarrow = 1.8$. That gives a spin polarization of 29% at this particular $\boldsymbol{k}$-point in a particular geometry. The data [7] from Ni(1 1 0) in Fig. 2 give a lower ratio of $A_\uparrow/A_\downarrow = 1.2$, resulting in a spin polarization of 9%. This polarization of 9–29% is to be compounded with the 6% spin polarization expected from the different size of the majority and minority spin Fermi surface (Eq. (11)). The resulting total polarization comes closer to the 23–33% observed in tunneling [32,72,73] particularly when considering a depolarization at higher temperature. (Our results are for 200 K, whereas the tunneling data were taken at much lower temperatures.) It remains to be explored how much the spin polarization varies for different locations on the Fermi surface of the s, p-band and how much of it is due to a spin-dependent photoemission matrix element [7]. We note that the area ratio $A_\uparrow/A_\downarrow$ is a pure bulk effect. It does not change when depositing a Cu overlayer or adsorbing residual gas [7].

A third element of a more accurate theory of spin-polarized tunneling [18–20] would be the inclusion of the matrix elements for tunneling and photoemission. The s, p-states with their more extended wave functions will dominate the matrix element in tunneling. The photoemission matrix element was calculated and found to contribute significantly to the spin polarization at E_F [7].

4. Outlook: fabricating wire and dot arrays by self-assembly

The idea of tailoring electronic states in nanostructures has been demonstrated in Section 3.1 for two-dimensional layer structures. Going down to one-dimensional wires and zero-dimensional dots one expects even a stronger effect on the density of states, such as $1/\sqrt{E}$ singularities (Fig. 3) and δ functions, respectively. It is difficult and slow to get down to the single-digit nanometer level by writing or lithography. For producing macroscopic amounts of such materials it would be desirable to find self-assembly techniques. A variety of methods are currently being tested. Here we give a progress report on an effort to utilize stepped Si surfaces [75,76] as templates for producing linear arrays [77,78] of stripes and dots. The idea is to develop a 'universal' fabrication method that allows the deposition of arbitrary materials (ferromagnets, noble metals, insulators) onto a substrate of choice, such as Si, borrowing as many techniques from Si microlithography as possible. The first step consists of preparing highly perfect step arrays on silicon, the second of decorating these steps with a mask material by self-assembly, and the third step of selective etching or deposition, for example by selective adsorption, chemical vapor deposition, or electroplating.

The first step has been highly successful: on the Si(1 1 1)7×7 surface it has been possible to create steps with only a single kink in 20 000 edge atoms by a straightforward annealing sequence [75,76]. As mask material, epitaxial CaF_2 has been tested. Depending on the coverage and growth temperature, CaF_2 grows in stripes or forms strings of nano-dots attached to the Si step edges [77,78]. These are typically 7 nm wide and 15 nm apart. Dot arrays with densities of 2 Teradots/inch^2 have been produced [77,78] which might become useful as masks for patterned magnetic storage media

[79]. The stripe spacing can be controlled by the miscut angle of the Si wafer, the stripe width by the CaF_2 coverage. Selective deposition of organic molecules has been demonstrated on CaF_2 stripe arrays [80], including nickelocene, a promising precursor for depositing carbon-and oxygen-free Ni by photolysis [81–83]. With silicon templates there are many other options for borrowing deposition and etching techniqes from silicon technology. Eventually, one could consider incorporating nanostructures into Si-based microdevices on the same chip.

Acknowledgements

This work was supported by the NSF under Award Nos. DMR-9400399, DMR-9624753, DMR-9632527, DMR-9704196, and DMR-9815416. It was partly conducted at the SRC, which is supported by the NSF under Award No. DMR-9531009.

References

[1] A series of articles on magnetoelectronics is published in: Phys. Today 48 (1995) 24–63. (For a current overview see G.A. Prinz in this issue of J. Magn. Magn. Mater.)
[2] L.M. Falicov, D.T. Pierce, S.D. Bader, R. Gronsky, K.B. Hathaway, H.J. Hopster, D.N. Lambeth, S.S.P. Parkin, G. Prinz, M. Salamon, I.K. Schuller, R.H. Victora, J. Mater. Res. 5 (1990) 1299.
[3] F.J. Himpsel, J.E. Ortega, G.J. Mankey, R.F. Willis, Adv. Phys. 47 (1998) 511.
[4] C. Tsang, R.E. Fontana, T. Lin, D.E. Heim, V.S. Speriosu, B.A. Gurney, M. Williams, IEEE Trans. Magn. 30 (1994) 3801.
[5] M.B. Stearns, J. Magn. Magn. Mater. 5 (1977) 167.
[6] M.B. Stearns, Phys. Today, April issue (1978) 34.
[7] K.N. Altmann, D.Y. Petrovykh, G.J. Mankey, N. Shannon, N. Gilman, M. Hochstrasser, R.F. Willis, F.J. Himpsel, to be published.
[8] D.Y. Petrovykh, K.N. Altmann, H. Höchst, M. Laubscher, S. Maat, G.J. Mankey, F.J. Himpsel, Appl. Phys. Lett. 73 (1998) 3459.
[9] F.J. Himpsel, Adv. Phys. 32 (1983) 1.
[10] F.J. Himpsel, Comments Cond. Mater. Phys. 12 (1986) 199.
[11] M. Bode, R. Pascal, R. Wiesendanger, Appl. Phys. A 62 (1996) 571.
[12] A. Davies, J.A. Stroscio, D.T. Pierce, R.J. Celotta, Phys. Rev. Lett. 76 (1996) 4175.
[13] R. Raue, H. Hopster, R. Clauberg, Phys. Rev. Lett. 50 (1983) 1623.
[14] E. Kisker, A. Schröder, M. Campagna, W. Gudat, Phys. Rev. B 31 (1985) 329.
[15] P.D. Johnson, Rep. Prog. Phys. 60 (1997) 1217.
[16] M. Donath, Appl. Phys. A 49 (1989) 351.
[17] R. Wiesendanger, Spin-polarized scanning tunneling microscopy, in: R. Wiesendanger (Ed.), Scanning Probe Microscopy, Springer, Berlin, 1998, p. 71 (Chapter 4).
[18] J.C. Slonczewski, Phys. Rev. B 39 (1989) 6995.
[19] J. Mathon, Phys. Rev. B 56 (1997) 11810.
[20] J.M. MacLaren, X.-D. Zhang, W.H. Butler, Phys. Rev. B 56 (1997) 11827.
[21] N.V. Smith, R. Lässer, S. Chiang, Phys. Rev. B 25 (1982) 793.
[22] G.J. Mankey, R.F. Willis, F.J. Himpsel, Phys. Rev. B 48 (1993) 10284.
[23] F.J. Himpsel, O. Rader, Appl. Phys. Lett. 67 (1995) 1151.
[24] O. Gunnarson, J. Phys. F 6 (1976) 587.
[25] F.J. Himpsel, Phys. Rev. Lett. 67 (1991) 2363.
[26] D.A. Papaconstantopoulos, Handbook of the Band Structure of Elemental Solids, Plenum Press, New York, 1986.
[27] T. Valet, A. Fert, Phys. Rev. B 48 (1993) 7099.
[28] P.M. Levy, S. Zhang, A. Fert, Phys. Rev. Lett. 65 (1990) 1643.
[29] R.Q. Hood, L.M. Falicov, Phys. Rev. B 46 (1992) 8287.
[30] J. Bass, W.R. Pratt, P.A. Schroeder, Comments Cond. Mater. Phys. 18 (1998) 223.
[31] J. Bass, W. Pratt, in this issue of J. Magn. Magn. Mater.
[32] R. Meservey, P.M. Tedrow, Phys. Rep. 238 (1994) 173.
[33] J.S. Moodera, J. Nowak, R.J.M. van de Veerdonk, Phys. Rev. Lett. 80 (1998) 2941.
[34] J. Moodera, G. Mathon, in this issue of J. Magn. Magn. Mater.
[35] I.A. Campbell, A. Fert, in: E.P. Wohlfarth (Ed.), Ferromagnetic Materials, Vol. 3, North-Holland, Amsterdam, 1982.
[36] Landolt-Börnstein, New Series III, 15a,b (1982) 139.
[37] S.Y. Hsu, A. Barthélémy, P. Holody, R. Loloee, P.A. Schroeder, A. Fert, Phys. Rev. Lett. 78 (1997) 2652.
[38] S.S.P. Parkin, Appl. Phys. Lett. 61 (1992) 1358.
[39] S.S.P. Parkin, Phys. Rev. Lett. 71 (1993) 1641.
[40] F.J. Himpsel, Phys. Rev. B 44 (1991) 5966.
[41] J.E. Ortega, F.J. Himpsel, Phys. Rev. B 47 (1993) 16441.
[42] C. Hwang, F.J. Himpsel, Phys. Rev. B 52 (1995) 15368.
[43] Dongqi Li, J. Pearson, J.E. Mattson, S.D. Bader, P.D. Johnson, Phys. Rev. B 51 (1995) 7195.
[44] J. Bass, Q. Yang, S.F. Lee, P. Holody, R. Loloee, P.A. Schroeder, W.P. Pratt, J. Appl. Phys. 75 (1994) 6699.
[45] A. Fert, T. Valet, J. Barnas, J. Appl. Phys. 75 (1994) 6693.
[46] A. Fert, S.-F. Lee, Phys. Rev. B 53 (1996) 6554.
[47] S.D. Steenwyk, S.Y. Hsu, R. Loloee, J. Bass, W.P. Pratt, J. Magn. Magn. Mater. 170 (1997) L1.
[48] B. Dieny, Europhys. Lett. 17 (1992) 261.
[49] B.A. Gurney, V.S. Speriosu, J.P. Nozieres, H. Lefakis, D.R. Wilhoit, O.U. Need, Phys. Rev. Lett. 71 (1993) 4023.
[50] B. Dieny, A. Granovsky, A. Vedyaev, N. Ryzhanova, C. Cowache, L.G. Pereira, J. Magn. Magn. Mater. 151 (1995) 378.

[51] W.P. Pratt, Q. Yang, L.L. Henry, P. Holody, W.-C. Chiang, P.A. Schroeder, J. Bass, J. Appl. Phys. 79 (1996) 5811. (Note that there are also results indicating that the change in the minority spin scattering could be an interface effect: S.S.P. Parkin, to be published).
[52] C. Guillot, Y. Ballu, J. Paigné, J. Lecante, K.P. Jain, P. Thiry, R. Pinchaux, Y. Pétroff, L.M. Falicov, Phys. Rev. Lett. 39 (1977) 1632.
[53] M. Iwan, F.J. Himpsel, D.E. Eastman, Phys. Rev. Lett. 43 (1979) 1829.
[54] F.J. Himpsel, P. Heimann, D.E. Eastman, J. Appl. Phys. 52 (1981) 1658.
[55] S.F. Alvarado, Phys. Rev. Lett. 75 (1995) 513.
[56] J.E. Ortega, F.J. Himpsel, Phys. Rev. Lett. 69 (1992) 844.
[57] J.E. Ortega, F.J. Himpsel, G.J. Mankey, R.F. Willis, Phys. Rev. B 47 (1993) 1540.
[58] D.M. Edwards, J. Mathon, R.B. Muniz, M.S. Phan, Phys. Rev. Lett. 67 (1991) 493.
[59] M.D. Stiles, Phys. Rev. B 48 (1993) 7238.
[60] D.D. Koelling, Phys. Rev. B 50 (1994) 273.
[61] P. Bruno, Phys. Rev. B 52 (1995) 411. (For an overview see M. Stiles in this issue of J. Magn. Magn. Mater.).
[62] Z.Q. Qiu, J. Pearson, S.D. Bader, Phys. Rev. B 46 (1992) 8659.
[63] R.K. Kawakami, E. Rotenberg, Ernesto J. Escorcia-Aparicio, Hyuk J. Choi, J.H. Wolfe, N.V. Smith, Z.Q. Qiu, Phys. Rev. Lett., submitted for publication.
[64] R. Wu, A.J. Freeman, J. Appl. Phys. 79 (1996) 6500.
[65] K. Garrison, Y. Chang, P.D. Johnson, Phys. Rev. Lett. 71 (1993) 2801.
[66] C. Carbone, E. Vescovo, O. Rader, W. Gudat, W. Eberhardt, Phys. Rev. Lett. 71 (1993) 2805.
[67] J.E. Ortega, A. Närmann, K.N. Altmann, W. O'Brien, D.J. Seo, F.J. Himpsel, P. Segovia, A. Mascaraque, E.G. Michel, J. Magn. Magn. Mater. 203 (1999) 126.
[68] M.G. Samant, J. Stöhr, S.S.P. Parkin, G.A. Held, B.D. Hermsmeier, F. Herman, M. van Schilfgaarde, L.-C. Duda, D.C. Mancini, N. Wassdahl, R. Nakajima, Phys. Rev. Lett. 72 (1994) 1112.
[69] S. Pizzini, C. Giorgetti, A. Fontaine, E. Dartyge, G. Krill, J.F. Bobo, M. Piecuch, Phys. Rev. Lett. 74 (1995) 1470. (For an overview see J. Stöhr in this issue of J. Magn. Magn. Mater.).
[70] Dongqi Li, J. Pearson, S.D. Bader, E. Vescovo, D.-J. Huang, P.D. Johnson, B. Heinrich, Phys. Rev. Lett. 78 (1997) 1154.
[71] W.P. Pratt, S.-F. Lee, Q. Yang, P. Holody, R. Loloee, P.A. Schroeder, J. Bass, J. Appl. Phys. 73 (1993) 5326.
[72] J.S. Moodera, R.J.M. van de Veerdonk, to be published.
[73] S.S.P. Parkin in this issue of J. Magn. Magn. Mater.
[74] A.V. Gold, J. Low Temp. Phys. 16 (1974) 3.
[75] J. Viernow, J.-L. Lin, D.Y. Petrovykh, F.M. Leibsle, F.K. Men, F.J. Himpsel, Appl. Phys. Lett. 72 (1998) 948.
[76] J.-L. Lin, D.Y. Petrovykh, J. Viernow, F.K. Men, D.J. Seo, F.J. Himpsel, J. Appl. Phys. 84 (1998) 255.
[77] J. Viernow, D.Y. Petrovykh, F.K. Men, A. Kirakosian, J.-L. Lin, F.J. Himpsel, Appl. Phys. Lett. 74 (1999) 12.
[78] D.Y. Petrovykh, J. Viernow, J.-L. Lin, F.M. Leibsle, F. K. Men, A. Kirakosian, F.J. Himpsel, J. Vac. Sci. Technol. A 17 (July/August 1999), in press.
[79] D. Lambeth, in this issue of J. Magn. Magn. Mater.
[80] H. Rauscher, T.A. Jung, J.-L. Lin, A. Kirakosian, F.J. Himpsel, U. Röhr, K. Müllen, Chem. Phys. Lett. 303 (1999) 363.
[81] J.V. Armstrong, A.A. Burk, J.M. Coey, K. Moorjani, Appl. Phys. Lett. 50 (1987) 131.
[82] D. Welipitiya, C. Waldfried, C.N. Borca, P.A. Dowben, N.M. Boag, H. Jiang, I. Gobulukoglu, B.W. Robertson, Surf. Sci. 418 (1998) 466.
[83] J.-L. Lin, H. Rauscher, A. Kirakosian, F.J. Himpsel, J. Appl. Phys., submitted for publication.